LUNAR RADIOACTIVE HEAT SOURCE DISTRIBUTION AND MAGNETIC FIELD GENERATION. M. Laneuville[1], J. Taylor[2], and M. Wieczorek[3]. [1]Earth-Life Science Institute, Tokyo Institute of Technology, Tokyo, Japan, [2]Hawai'i Institute of Geophysics and Planetology, University of Hawai'i, Honolulu, HI 96822, USA, [3]Laboratoire Lagrange, Observatoire de la Côte d'Azur, Nice, France.

Introduction. The Moon possesses a notable enrichment in thorium and other incompatible elements (KREEP) on the nearside in a region called the Procellarum KREEP Terrane (PKT). The exact nature of the relationship between this enrichment and the highly correlated volcanic activity is debated, but it has been shown that different distributions of heat sources will lead to drastically different long term evolutions, with influence on magnetic field generation [1,2], crater morphology [3], true polar wander [4], and magmatism [e.g. 5-7].

Here we use updated radioactive heat source budget estimates as well as insights from remanent magnetization of the crust to test different scenarios of heat source distribution. In particular, we consider the effect on the cooling rate of the crust, which has implication for both remanent magnetization and radiometric dating of lunar samples.

Heat source distribution. We use an average crustal thickness of 26.3 km for the PKT from [8] and several assumptions for its internal structure and that of the underlying mantle.

We consider two average concentrations for the highlands crust thorium content: 1 ppm and 0.18 ppm. The first case corresponds to the average surface observation from the Lunar Prospector GRS [9] and assumes it is representative of the whole crust, while the latter assumes it is representative of the upper 5 km only and the remainder of the crust is FAN with 0.05 ppm thorium (average of 5 FAN rocks from the literature). Similarly, we consider two possible thorium concentrations for the PKT region: 5.7 ppm and 8.2 ppm. The former corresponds to the observed surface average, while the latter corresponds to the mean concentration in Apollo mafic impact melt breccias [10], which is a realistic maximum concentration.

In addition, we consider different structures for the PKT region itself. The existence of a magnetic low in the inner part of this region suggests that the heat source distribution is not uniform within the PKT itself [11,12]. In model 5, only an "inner" PKT region has a concentration of 8.2 ppm and corresponds to the area of the magnetic low (D = 1712 km), while the outer PKT has a concentration of 4 ppm, to keep the total PKT thorium content constant. In all other models, the PKT has a uniform concentration of 5.7 ppm.

In all models, the mantle concentration is chosen to be consistent with the expected bulk silicate content of 79.5 ppb thorium [8]. Models 1 to 3 are uniform in thorium concentration. Models 4 and 5 are enriched in mantle thorium concentration beneath the PKT because they assume that mare basalt source regions reflect elevated thorium due to sinking of late-stage (Th- and Ti-rich) magma ocean products. Assuming between 5% and 10% partial melting, we estimate the thorium concentration to be about 55 ppb. The concentration in the rest of the mantle is then calculated by mass balance The concentrations for all layers is summarized in Table 1.

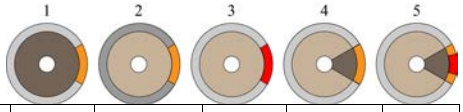

	M1	M2	M3	M4	M5
Highlands	0.18	1	0.18	0.18	0.18
PKT	5.7	5.7	8.2	5.7	4
Inner PKT					8.2
Highlands	0.039	0.0074	0.025	0.038	0.04
PKT	0.039	0.0074	0.025	0.055	0.055

Table 1. Thorium contents of the different regions in ppm (Th/U = 3.68, K/U = 1250). Inner PKT is the innermost PKT region. Gray areas are crust and white are mantle concentrations.

Thermal evolution model. We use the 3D thermochemical convection code Gaia already used in [5], changing only the initial distributions of radioactive heat sources. As an initial set of parameters, the core is 330 km and possesses 4 wt.% S as an alloying element, the melting curve and reference viscosity correspond to that of a dry peridotite, and there is no density contrast in the mantle other than that generated by melting (Boussinesq approximation). All models are run with a fixed 10 km radial resolution.

Model constraints and predictions. We first test the validity of the different models by looking at melt generation. Crater counting techniques combined with samples dating have set the range of mare basalt ages from about 4 to 1 Ga on the nearside, and 3 to 2.5 Ga on the farside [13]. Total extruded volume is estimated to be around 5×10^6 km^3, with an extrusive to intrusive volume ratio between 1:2 and 1:10 [13]. We keep in mind that those ratios were derived for the Earth, and mostly use the range of ages as constraints to the models.

We found that only model 1, 4 and 5 can sustain a continuous volcanic activity up to 2 Ga ago, which is the closest those models get from the observations. Similarly, those models generate continuous volcanic activity up to 2.5 Ga go on the farside, while models 2 and 3 – with the lowest thorium concentration in the mantle – sustain only a few 100 million years of volcanism. In terms of volume, model 1, 4 and 5 require about 1:100 extrusive to intrusive volcanic ratio in order to match the extruded 5 x 10^6 km^3 estimate.

Another way to constrain the models is to compare the predicted surface heat flow at the present day with known values. Fig. 1 shows a longitudinal profile centered on the PKT region. Measurements are from the heat flow probe installed during the Apollo 15 and 17 missions, and remote sensing radiometric analysis of permanently shadowed areas near the north pole from the Diviner instrument onboard the LRO mission [e.g., 14]. Model 3 predicts a strong surface heat flow within the PKT, which is inconsistent with the observations. All other models fit reasonably well the observations. In particular, model 5 predicts a strong heat flow in the inner part of the PKT region. This prediction may be testable by looking at relative crater morphologies for instance [e.g., 13].

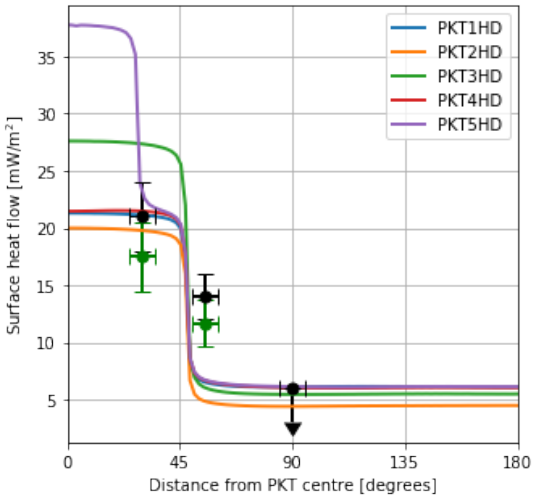

Figure 1. Surface heat flow at the present day predicted by the different models described in Table 1. The black disks are constraints from Apollo 15, 17 and DIVINER radiometer, respectively (from left to right). The green disks below Apollo estimates take into account the heat focusing effect discussed in [15].

Finally, the strong lateral variations in heat source distribution also imply large differences in cooling rate in the crust. The time required for a fraction of the crust to cool down below a given isotherm may vary by a few 100 million years depending on location. Most closing temperatures for minerals used in radiometric dating are between 800 and 1000 K [16], it is therefore possible that some of the ages obtained record different ages than expected. As an example, Figure 2 shows the depth of the 800 and 1000 K isotherm below the PKT and the antipodal point using the evolution obtained with model 1.

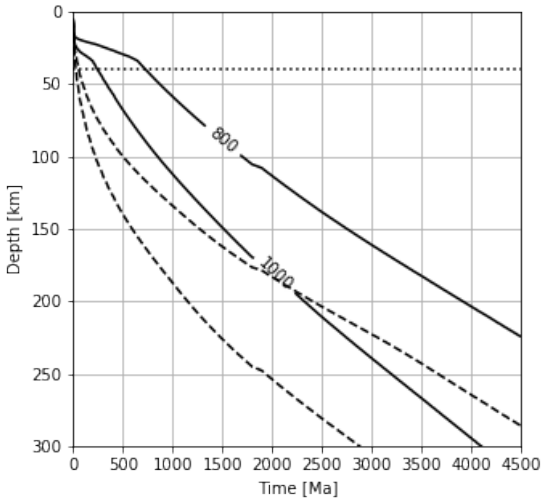

Figure 2. Two isotherm depths as a function of time within the PKT (solid line) and farside (dashed), for model 1. The dotted line is at constant 40 km depth.

Concluding remarks. Understanding the distribution of KREEP material in the lunar crust is key to unravelling the Moon's early history. We used thermal model to test new distributions based on updated crustal thickness from GRAIL gravity data and PKT region structure inferred from remanent magnetization data.

The results indicate that the concentration of KREEP visible in the crust of the PKT extends to the mantle beneath it. In addition, the thermal models are consistent with a higher KREEP content in the central, low magnetism region of the PKT and suggesting that the PKT is radially zoned, at least in the crust.

References. [1] Laneuville et al. (2014) *EPSL*, [2] Scheinberg et al. (2015) *Icarus*, [3] Miljkovic et al. (2013) *Science*, [4] Siegler et al. (2016) *Nature*, [5] Laneuville et al. (2013) *JGR*, [6] Zhang et al. (2013) *JGR*, [7] Evans and Zuber (2014) *JGR*, [8] Taylor and Wieczorek (2014), *Phil. Trans. R. Soc. A.*, [9] Lawrence et al. (2007) *GLR*, [10] Korotev (2000) *JGR*, [11] Wieczorek (2018) *JGR*, [12] Wieczorek et al. (2018), *LPSC 49*, [13] Kamata et al. (2013) *JGR*, [14] Paige and Siegler (2016) *LPSC 47*, [15] Warren and Rasmusen (1987) *JGR* [16] Dodson (1973) *Contrib. Min. Petrol.*